Faculty of Engineering

University of Southern Denmark

A study on physical models representing vibration responses of hanger cables in the Great Belt Bridge

Profiling project

Authors:

456167 Liv Obbekær

453035 Julie Lynge Madsen

Supervisor:

Luis David Avendaño-Valencia

May 31, 2022

Abstract

Monitoring bridges has been an important tool for many years to understand the condition of a bridge, and it is important because it can prevent damage and reduce the risk of human losses. In this study, the focus is to develop and investigate three different physical models representing vibration responses of the hanger cables in the Great Belt Bridge in normal operational conditions, because these components are subject to high vibration and loads. An approach for a model updating strategy is developed, and a comparative analysis of the three models is made to select the best-suited physical models for developing a Structural Health Monitoring strategy for the hanger cables. An iterative non-linear optimization method with the natural frequencies as the characteristic quantities is used for the model updating of one model, while for the two other models, model updating is conducted by solving for the axial load directly. The comparative analysis is conducted based on a plot illustrating the trend of the three models. It is concluded that the trend of the physical models is approximately the same, making it possible to switch from one model to the other with a deterministic correction. The updated results show good agreement between the physical and the actual model, and the simplest model, in relation to computational effort, can be chosen as the best-suited physical model and it is concluded that it is a pinned-pinned beam model.

Table of Contents

List of Figures

List of Tables

Nomenclature

Important symbols and their meanings used in this study are explained below.

List of notations

Latin notations

a = Acceleration

A = Constant

A = Area

B = Constant

c_1, c_2, c_3, c_4 = Constant

C = Constant

d = Distance between hanger pairs

D = Constant

E = Young's modulus

f = Distributed load

F = Force

$G_{ij}(j\omega)$ = Power Spectral Density matrix

$H(j\omega)$ = Frequency Response Function matrix

I = Moment of inertia

l = Length of hanger cable

L = Length of hanger cable

m = Mass

M, M_0 = Moment

n = An integer

N = Block size

$Nover$ = Number of overlapping samples

P = Axial force

r, r_1, r_2 = Root

$R(p)$ = Difference between estimated and measured quantity

$T(t)$ = A function of time

V = Shear force

w = Displacement

$W(x)$ = Shape function

x_0 = Initial guess

x_{n+1} = Point in Newton-Raphson method

Greek notations

θ = Constant, angular displacement

ρ = Density

$\omega, \omega_n, \omega_{n,model}, \omega_{n,measure}$ = Natural frequency

Special symbols and abbreviations

BC = Boundary Condition(s)

DOF = Degree of Freedom(s)

EA = Evolutionary Algorithm(s)

FE = Finite Element

FRF = Frequency Response Function

GA = Genetic Algorithm(s)

LTI = Linear Time Invariant

PSD = Power Spectral Density

PSO = Particle-swarm-optimization

$\| \quad \|$ = Determinant

1 Introduction

Monitoring of structures has been performed for several years now. Monitoring is important because it helps to understand the condition of the structure. This can prevent damage and undesirable situations. A structure that is often being monitored is a bridge, and a good example of that is the Great Belt Bridge. The benefits of monitoring range from quick detection of damages and reduced operations and maintenance costs to the reduction of the risk of catastrophic damage and human loss. The knowledge of a bridge's condition cannot be used for anything unless the bridge's normal condition is known. Otherwise, it is not possible to conclude anything from a comparison. One way to get knowledge about the bridge's condition is by measuring the vibration of the stay cables on the bridge. In this study, the focus is on the hanger cables of the Great Belt Bridge, as these components are subject to high vibration and loads, and thus are more prone to fatigue damage. These high vibrations are being monitored but in order to tell the condition of the hanger cable, a well-developed physical model is needed.

Therefore, this study aims to develop and compare different physical models representing the vibration response of the hanger cables of the Great Belt Bridge in normal operational conditions and establish a model updating strategy that can be used for monitoring the hanger cable loads in the Great Belt Bridge. Furthermore, this study aims to form the basis of selecting the best-suited physical model for the purpose of developing a Structural Health Monitoring strategy for the hanger cables.

The physical models are developed as continuous mechanics models of the hanger vibrations, which are, in a subsequent step, adjusted to the measured vibration characteristics obtained from sensors attached to the cables. From this, a comparative analysis of the different physical models is made.

The codes that form the basis of this study can be accessed by GitHub by the following link: https://github.com/LivogJulie/Profiling-project

1.1 State of the Art

Mathematical models are used to describe the behaviours of real structures in their operational environment. The model must produce outputs which are representative of the structure's response. Often, it turns out that the outputs produced by the model are quite different from the measurements. To choose the most proper updating quantity and optimisation method a state-of-the-art review on updating physical models from measured data is conducted.

1.1.1 Characteristic quantities for model updating

Often, when evaluating a structural model's capacity to predict the actual response of the structure, it is based on a comparison between experimental quantities from the vibration test and estimated quantities from the model. Quantities used for this can be for example natural frequencies and mode shapes, as they give a solid foundation for determining if the model's prediction accurately represents the structure's overall dynamic response.

As seen in the work of Guo et al. [1] the natural frequency can be used as an updating quantity to validate if the model is identical to the measurements. In this study, the natural frequency provides the global information of the structure and is used to guarantee the accuracy of the modal properties of the global model. The article states that, for natural frequencies, the absolute or relative errors between the experimental and the analytical frequencies can be directly used as the objective function for dynamic FE model updating. However, the article also states that if the mode shape is used alone to formulate the objective function some useful structural information may be neglected. This is due to mode shapes not being identified accurately and as a result, the updated model can also be less accurate.

Another technique is to use data directly in the frequency domain. In this way, modal analysis, which is necessary for obtaining modal parameters, can be avoided. In the frequency domain, a method is to approximate the *Power Spectral Density* (PSD) of the structural response, which for a *Linear Time Invariant* (LTI) system can be calculated as follows:

$$G_{yy}(j\omega) = H(j\omega)^{*} G_{xx}(j\omega) H(j\omega)^{T} \tag{1}$$

Where $G_{xx}(j\omega)$ is the input PSD matrix, $G_{yy}(j\omega)$ is the output PSD matrix, and $H(j\omega)$ is the *Frequency Response Function* (FRF) matrix [2]. To make the input PSD matrix when the excitation, $G_{xx}(j\omega)$, is unknown, a white noise excitation is assumed, and to make the FRF matrix, the *Degree of Freedoms* (DOFs) in which the structure is excited must be known.

The PSD is used as a model updating quantity in the work of Pedram et al. [3], where the viability of damage detection using PSD of structural response both numerically and experimentally is investigated. In the study, an FE model is developed and assumptions of excitation in certain DOFs are made. These assumptions of excitation lead to the auto spectral and cross-spectral density of the responses.

The model updating quantity can also be the FRF matrix, which can be used directly to update the model without the need to extract natural frequencies and mode shapes. The study of Prendergast et al. [4] investigates an FRF FE model updating approach applied to two test piles. From an impact test on a test pile, an FRF is obtained, and afterwards, a numerical model of the system is developed with initial estimates of soil mass and stiffness. Afterwards, these properties are updated to match the experimental FRF with the numerical model.

1.1.2 Optimization strategies for model updating

Model updating is necessary when the estimated quantity from the model and the quantity from the measurements do not correlate. A parameter selection is conducted and based on the selected parameters an objective function is minimized. Often, this objective function is non-linear with respect to the updating parameters, therefore, iterative non-linear optimization methods can be used to minimize the objective function.

Traditional optimization methods start from an arbitrarily chosen initial solution and with each iteration, it converges to a locally optimal solution. Search direction and step length are the two important parameters to be determined before performing optimization [5]. There are several traditional optimization methods available, and they are broadly divided into two groups: Direct search methods and gradient-based methods [6]. The direct search methods include among others the random search method and the pattern search method. The direct search methods do not require any information about the gradient of the objective function, and they can be used if the objective function is not differentiable or if it is not continuous [7]. The steepest descent method and the conjugate gradient method, on the other hand, are two gradient-based methods. In these methods, the search direction is decided on basis of the gradient of the objective function.

Gradient-based algorithms often lead to a local optimum, whereas non-gradient algorithms usually converge to a global optimum [8]. Therefore, when using gradient-based methods, it is necessary to investigate, if the correct optimum is obtained. Gradient-based methods are not well-suited for objective functions featuring discontinuities. As a result, the need for non-traditional optimisation methods became apparent [5]. *Evolutionary Algorithms* (EA) are a category containing non-traditional optimisation methods, including *Genetic Algorithms* (GAs) and *Particle-Swarm-Optimization* (PSO).

EA are search methods based on Darwinian evolution that capture global solutions to complex optimization problems. The EAs require no information about the gradient, and they can escape from local minima [9].

The most representative method for model updating is the GA [10]. The GA does a directional and probabilistic search without using the derivatives, and the advantage of this is that the GA can solve optimization problems that include discontinuity and non-convex regions. The GA is a probabilistic population-based technique used to find a solution to a problem from a population of possible solutions [11]. The GA is inspired by Darwin's theory of survival of the fittest. The GAs develops better and better solutions by having the possible solutions to the problem in a data structure of a fixed form and gradually transforming them. A genetic algorithm, unlike many other optimization methods, converges to a global optimal solution [12]. Ribeiro et al. [13] successfully used a genetic algorithm in the work of calibrating a numerical model of a track section over a railway bridge based on dynamic tests. Here, the method was efficient and robust in estimating several track numerical parameters.

The main drawback of the GA method is the complexity of its implementation, therefore, the PSO method was introduced as an alternative. PSO method is a population-based approach that was inspired by a mathematical description of the swarming of birds. PSO solves a problem by generating a population of candidate solutions, which are referred to as particles, and moving them around in the search space. Some of the advantages of PSO are that it does not require the calculation of the objective function derivatives and it is easy to execute. It is also effective for finding global optimum but the disadvantage of the PSO method is that it is not good at searching for a local solution and therefore it may converge prematurely [11]. In the work of Alkayam et al. [10], they compared the performance of PSO to other EA methods to update a finite element model, where the results showed that PSO performed better than GA.

In the category of probabilistic model updating techniques is the Bayesian approach. It is a probabilistic model updating technique that is based on Bayes' Theorem. Bayes' Theorem combines prior information (previous knowledge) about a parameter with evidence (observations) from new information coming from observed data. The model is updated by using the observations to update the probability that a hypothesis may be true. The main problem then is to obtain the updated probability model (posterior). The updating process is based on the Bayes theorem, but the actual implementation will differ according to the type of probability model selected for the prior and evidence. While the multivariate normal model can simplify a lot the updating procedure, it might constrain too much the obtained distribution. On the other hand, more flexible probability models can be used, nonetheless requiring Monte Carlo approaches for updating. Monte Carlo approaches are often used to solve the Bayesian methods [11].

2 Methodology

In the following, the overall procedure of this study will be covered. Afterwards, the different subjects will be elaborated on.

2.1 Overview of essential steps in the study

An overview of this study is created to clarify the essential steps and obtain a bigger picture of the process. The overview is made with a flow chart which can be seen in Figure 1.

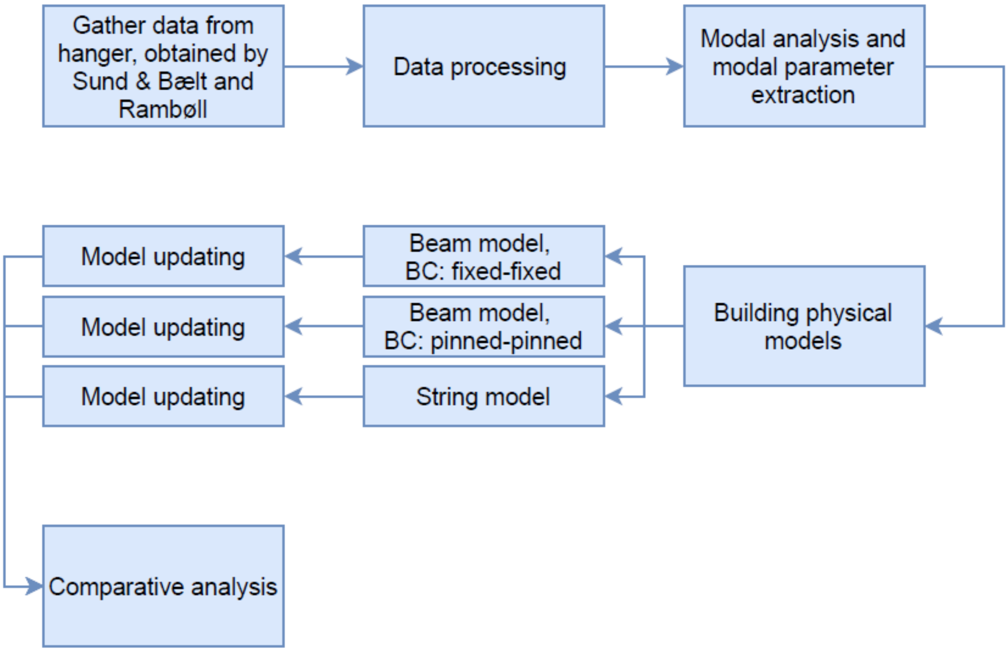

Figure 1 - Overview flow chart of essential steps

The methodology for every stage in the process shown in the flow chart will be elaborated on in the following sections.

2.2 Presentation of hanger monitoring data

The Great Belt Bridge is a suspension bridge with vertical hangers. In Figure 2, the upper end of one of the hanger cables is shown. The upper end of the hanger is fixed to the main cable by a pin connection, which makes it possible for the bridge to move in the lateral direction.

Figure 2 - Upper end of the hanger

To the left in Figure 3 below, the lower end of the hanger cable is shown. The lower end of the hanger cable connects the steel wires from the hanger in an anchor pipe, which can be seen in the right part of Figure 3. Furthermore, in the left picture of Figure 3, it can be seen that lateral supports called Dellner Dampers are added to the hanger pair. These are installed to reduce cable vibration.

Figure 3 - Lower end of the hanger (left) and anchor pipe (right)

In this study, the physical models are developed by assuming fixed-fixed and pinned-pinned *Boundary Conditions* (BCs). These two types of BCs are chosen because it is known that the hanger cable is fastened at both ends, and therefore two types of fastened BCs are investigated.

The data from the Great Belt Bridge used in this study is gathered by Sund & Bælt’s Structural Health Monitoring system. The data is collected from sensors that are placed on the hangers on the Great Belt Bridge. The sensors used are accelerometers measuring in the longitudinal direction, which is parallel to the length of the bridge, and the transverse direction, which is perpendicular to the length of the bridge. In this study, the accelerometers used are the ones placed closest to the pylon and the accelerometers are placed 4,5 meters over the road level. The reason the accelerometer closest to the pylon is chosen is that in the future, it would be interesting to look for vortex shedding, which would mostly occur at the hanger closest to the pylon. The location of the accelerometer used to collect the data can be seen in Figure 4 where it is indicated with a red arrow.

Figure 4 - Position of the accelerometer on the Great Belt Bridge

The data provided by Sund & Bælt has a sampling frequency of 25 Hz. This study is made based on data from 24 hours, which means this study is based on 2,160,000 sample points.

Before further analysis, some preprocessing of the data given by Sund & Bælt has to be made. Both the data obtained in the transverse and longitudinal directions are used to create a PSD plot. The PSD plot is computed with Welch's PSD estimate. The parameters used in Welch's estimator can be seen in Table 1.

Table 1 - Parameters used for Welch's PSD estimate

Total length of signal	$2{,}160{,}000\ samples = 24\ hours$
Sampling frequency	$25\ Hz$
Block size	$N = 2048\ samples = 81.9\ sek$
Window type	Hanning window
Number of overlapping samples	$nover = \frac{3 \cdot N}{4}$

The PSD made from these parameters can be seen in Figure 5.

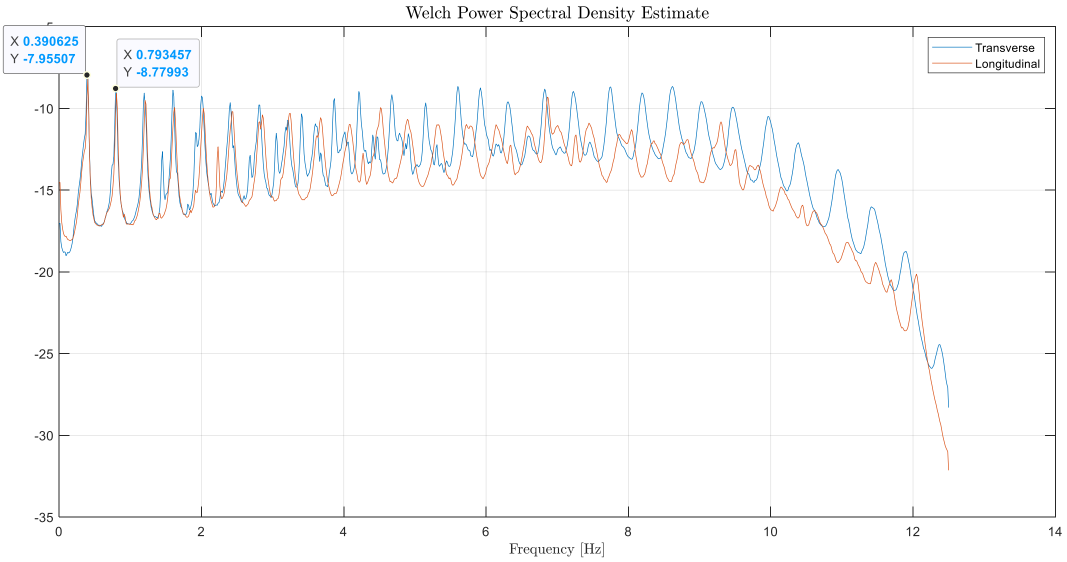

Figure 5 - PSD of transverse and longitudinal vibration of one day

When the PSD is obtained a modal analysis followed by a modal parameter extraction is made. This is done by peak picking the first natural frequency and reading off the value of 0.39 Hz. This value for the natural frequency is used later in the study to update the physical models.

The physical models are developed using basic structural properties of the hanger closest to the pylon provided by Rambøll Danmark A/S. The structural properties can be seen in Table 2:

Table 2 - Basic structural properties of hanger closets to the pylon

Hanger	147.2
Length [m]	177.168
Mass [kg/m]	51.6
Young's modulus [GPa]	160
Diameter [mm]	98

In the following section, the derivation for the shape function used in the physical models is made.

2.3 Derivation of shape function and frequency equation for physical models

The physical models are made to describe the data given by Sund & Bælt with a mathematical model. In this study, three different physical models will be investigated. This is done to investigate if one of the models fits the data better than one of the other models. Two of the models are axially loaded beams where one model is modelled with pinned-pinned BCs and the other beam model is modelled with fixed-fixed BCs. The last physical model is a string model with fixed-fixed BCs. Before it is possible to look at the models with specific BCs the shape function for the axially loaded beam and the shape function for the string model must be found.

2.3.1 Transverse vibration of a string under tension

To find the shape function for the string model, a differential element is first considered, which can be seen in Figure 6 [14].

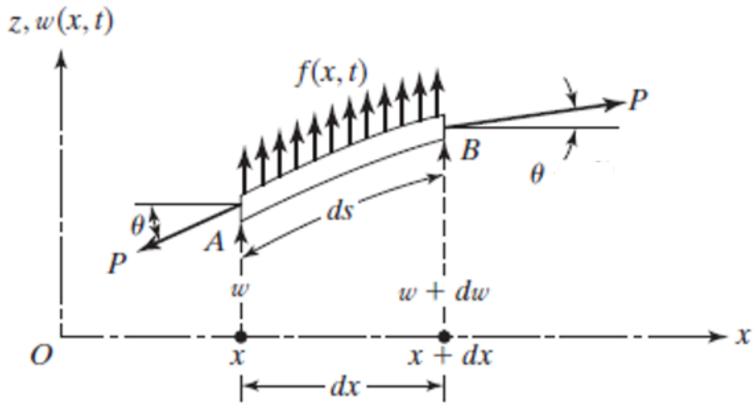

Figure 6 - Differential element of a vibrating string

This differential element has the length ds and has a distributed load perpendicular to the length of the string called $f(x,t)$. A horizontal line on each side of the element parallel to the x-axis is drawn to indicate the angle between this line and the tensile force P, which is also added on each side of the differential element. The left edge of the differential element is located at x and the right edge is located at $x + dx$. Newtons' second law is now applied to the differential element.

$$\sum F = ma \tag{2}$$

Where the mass of each differential section of the string, m, can be described as the density, ρ, times the distance, dx. The reason that the mass can be described in this way is that the density used is mass per unit length. From Newton's second law it is known that the mass is multiplied by the acceleration. To get the acceleration the displacement is investigated. The displacement of interest is in the z-direction, where transverse displacement occurs, the displacement is called w. The acceleration can be described as the second derivative of the displacement in relation to time, $\frac{\partial^2 w}{\partial t^2}$. This means that the mass multiplied by the acceleration can be described as:

$$ma = \rho dx \frac{\partial^2 w}{\partial t^2} \tag{3}$$

This expression is now set equal to the sum of the transverse loads. The sum of the transverse load is:

$$\sum F = f dx + (P) \cdot \sin(\theta) \mid_{x+dx} - P \cdot \sin(\theta) \mid_{x} \tag{4}$$

The first load that is present is the distributed load, *f*. The distributed load on the element is described as $f(x,t) \cdot dx$. The reason for this is that the load f is per unit length. Then the transverse component of the force, P, is added. The two forces have opposite signs because they point in opposite directions. The expression for the transverse forces and the mass times the acceleration is set equal to each other.

$$\rho dx \frac{\partial^2 w}{\partial t^2} = f dx + (P) \cdot \sin(\theta) \mid_{x+dx} - P \cdot \sin(\theta) \mid_{x} \tag{5}$$

The equation is now divided by the distance dx.

$$\rho \frac{\partial^2 w}{\partial t^2} = f + \frac{(P) \cdot \sin(\theta) \mid_{x+dx} - P \cdot \sin(\theta) \mid_{x}}{dx} \tag{6}$$

The limit where dx is going towards zero is now found.

$$\lim_{dx \to 0} \rho \frac{\partial^2 w}{\partial t^2} = f + \frac{(P) \cdot \sin(\theta) \mid_{x+dx} - P \cdot \sin(\theta) \mid_{x}}{dx} \tag{7}$$

This result is the following expression:

$$\rho \frac{\partial^2 w}{\partial t^2} = f + \frac{\partial}{\partial x}(P \cdot \sin(\theta)) \tag{8}$$

This result is obtained because the term divided by the differential length dx is the definition of a derivative.

To reduce the expression more, it is investigated what happens when small displacements are assumed as it is in this case. The differential element is drawn with the length ds and with its *x* and *z* components as seen in Figure 7.

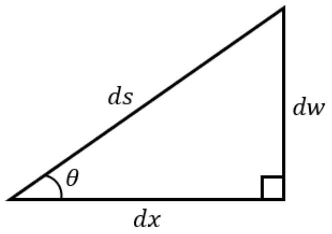

Figure 7 - Differential element

For this drawing, the following is known from trigonometry.

$$\sin(\theta) = \frac{dw}{ds} \qquad \tan(\theta) = \frac{dw}{dx} \tag{9}$$

If small displacements are assumed, as in this case, dw or θ will be very small, and then the lengths ds and dx are approximately equal. Furthermore, for small displacements the following can be obtained:

$$if\ \theta \ll 1 \Rightarrow \sin(\theta) \simeq \tan(\theta) = \frac{dw}{dx} \tag{10}$$

This means if the angle θ is very small then sin (θ) is approximately equal to θ which is approximately $\tan(\theta)$ and $\tan(\theta)$ we already have an expression for. This means that for small displacements $\sin(\theta)$ can be approximated as $\frac{dw}{dx}$. This expression is substituted into equation (8).

$$\rho \frac{\partial^2 w}{\partial t^2} = f + \frac{\partial}{\partial x}\left(P \cdot \frac{\partial w}{\partial x}\right) \tag{11}$$

The assumption is now that P is constant which is a fine assumption because P is the total tension in the string, and the tension is constant. Furthermore, the differential element is not moving in the horizontal direction and therefore the loads on each side are balanced and therefore P is constant. This means that we can rewrite equation (11) into the following:

$$\rho \frac{\partial^2 w}{\partial t^2} = f + P \cdot \frac{\partial^2 w}{\partial x^2} \tag{12}$$

The next step is to look at the case for free vibrations which means $f = 0$. This results in the following equation.

$$\rho \frac{\partial^2 w}{\partial t^2} = P \cdot \frac{\partial^2 w}{\partial x^2} \tag{13}$$

This equation is rewritten into the wave equation.

$$\frac{\partial^2 w}{\partial t^2} = c^2 \cdot \frac{\partial^2 w}{\partial x^2} \tag{14}$$

Where $c = \sqrt{\frac{P}{\rho}}$. The equation is now a second-order partial differential equation. The equation is both second order in time and space. The tension, P, acts like a stiffness in this case and this is the reason that the string is able to vibrate. Because the equation is both dependent on time and space, this is added to equation (14).

$$\frac{\partial^2 w}{\partial t^2}(x,t) = c^2 \cdot \frac{\partial^2 w}{\partial x^2}(x,t) \tag{15}$$

Then the method separation of variables is used. Here, w, which is dependent on both time and space, is rewritten into a part dependent on time and a part dependent on space. This means the following is obtained.

$$w(x,t) = W(x) \cdot T(t) \tag{16}$$

The solution for $W(x)$ and $T(t)$ is the following [14]:

$$W(x) = A\cos\left(\frac{\omega x}{c}\right) + B\sin\left(\frac{\omega x}{c}\right) \tag{17}$$

$$T(t) = C\cos(\omega t) + D\sin(\omega t) \tag{18}$$

To describe the mode shape, it is only the shape function that is necessary, therefore, the time-dependent part is not used in this study. Therefore, equation (17) is only investigated in this study.

2.3.1.1 Frequency equation

To find an equation for the natural frequency the BCs must be known. In this study, the fixed-fixed BC has been chosen for the string because the hanger cables on the Great Belt Bridge cannot move at the ends. If a pinned-pinned BC was chosen, then the pin would move in a perpendicular direction in relation to the string and any movement at the ends is not acceptable. For a fixed-fixed string, the BCs will look like the following: $w(0,t) = w(l,t) = 0$ for all time $t \geq 0$ and only the space-dependent part is interesting therefore the following BCs are used.

$$W(0) = 0 \tag{19}$$

$$W(l) = 0 \tag{20}$$

The first BC is inserted into equation (17).

$$W(0) = A\cos\left(\frac{\omega \cdot 0}{c}\right) + B\sin\left(\frac{\omega \cdot 0}{c}\right) = 0 \Rightarrow W(0) = A = 0 \tag{21}$$

From this, it can be concluded that A must be zero to fulfil the equation. This means the equation of $W(x)$ looks like the following:

$$W(x) = B\sin\left(\frac{\omega x}{c}\right) \tag{22}$$

The second BC is now used.

$$W(l) = B\sin\left(\frac{\omega l}{c}\right) = 0 \tag{23}$$

The constant B cannot be zero because then the result would be a trivial solution, and a non-trivial solution is desired therefore the following must be valid.

$$\sin\left(\frac{\omega l}{c}\right) = 0 \tag{24}$$

$\sin\left(\frac{\omega l}{c}\right)$ can be zero if $\frac{\omega l}{c} = n\pi$. Here, ω is the natural frequency, and the natural frequency can be isolated.

$$\frac{\omega_n l}{c} = n\pi \;\;\Rightarrow\;\; \omega_n = \frac{n\pi c}{l}, \qquad n = 1,2,\ldots \tag{25}$$

Hereby an equation for the natural frequency is obtained for the string model.

It is desired to find an expression for the tension, P, in the string. This is because the equation for the axial load, P, should be used to perform the model updating. This is done by inserting $c = \sqrt{\frac{P}{\rho}}$ in the equation for the natural frequency in equation (25) and solving for the axial load, P.

$$\omega_n = \frac{n\pi c}{l} \;\Rightarrow\; \omega_n = \frac{n\pi\sqrt{\frac{P}{\rho}}}{l} \;\Rightarrow\; P = \frac{\omega_n^2 L^2 \rho}{\pi^2 n^2} \quad , \qquad n = 1,2,\ldots \tag{26}$$

In this way, an expression for the tension, P, in the string as a function of density, length, and natural frequency is found, and equation (26) can be used to perform model updating.

2.3.2 Transverse vibration of axially loaded Bernoulli-Euler beam

A string does not account for bending stiffness, which results in cable failures due to fatigue caused by alternating bending [14]. Beam models consider bending stiffness, therefore, a beam model is also developed. To be able to model an axially loaded beam with both fixed-fixed and pinned-pinned BCs the shape function for an axially loaded beam must be found. An axially loaded beam can be seen in Figure 8 below [15].

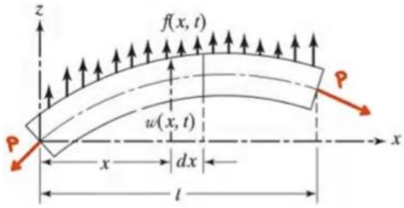

Figure 8 - Differential element of an axially loaded beam

First, a differential element is considered. This element has a shear force on each side V and $V + dV$. It also has a moment on each side which is opposite of each other. There is a distributed load, *f*, which is a load per unit length acting across the elements. The length of the element is *dx*. This can be seen in Figure 9 below [15].

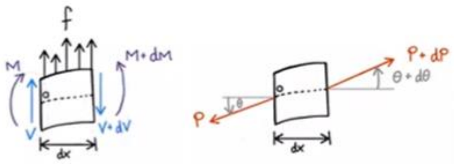

Figure 9 - Differential element 1 (left) and differential element 2 (right)

To get an axially loaded beam, the model for the string under tension is investigated. This element has a force, *P*, on one side and $P + dP$ on the other side. *P* is defined as a tensile load. Newton's second law is applied to the differential element in the *z*-direction. The forces are summed.

$$\sum F = ma \tag{27}$$

First, differential element 1 in Figure 9 is considered. Here, two forces are present: *V* in the vertical direction pointing upwards and $V + dV$ pointing downwards. Furthermore, the force, *f*, due to the distributed load is also present in differential element 1. Differential element 2 have components of, *P*, in the vertical direction. This results in the following equation.

$$-(V + dV) + f dx + (P + dP)\sin(\theta + d\theta) - P\sin(\theta) = \rho A dx \frac{\partial^2 w}{\partial t^2} \tag{28}$$

The equation is set equal to the mass of the differential element. This mass is equal to density times volume (ρV), where the volume is the cross-sectional area times the length, *dx*.

A moment balance around the point "o" is taken. The assumption that there is no rotation of the cross-sections is made, therefore the sum of the moments must equal zero.

$$\sum M_0 = 0 \tag{29}$$

From the Bernoulli-Euler beam, there are two contributions which are M and the $M + dM$. It is assumed that the counterclockwise direction is the positive direction. The distributed load is made into a point load acting at the midway point, which also results in a moment.

$$(M + dM) - M - (V + dV)dx + fdx\frac{dx}{2} = 0 \tag{30}$$

A small displacement assumption is made. For small deflections the following is valid:

$$\sin(\theta + d\theta) \backsimeq \theta + d\theta = \theta + \frac{\partial\theta}{\partial x}dx = \frac{\partial w}{\partial x} + \frac{\partial^2 w}{\partial x^2}dx \tag{31}$$

Here $\theta + \frac{\partial\theta}{\partial x}dx$ is the first-order Taylor approximation of $\theta + d\theta$ and theta can be described as $\theta = \frac{\partial w}{\partial x}$.

Substituting equation (31) into equation (28).

$$-\frac{\partial V}{\partial x}dx + fdx + \left(P + \frac{\partial P}{\partial x}dx\right)\left(\frac{\partial w}{\partial x} + \frac{\partial^2 w}{\partial x^2}dx\right) - P\frac{\partial w}{\partial x} = \rho A dx\frac{\partial^2 w}{\partial t^2} \tag{32}$$

By expanding the equation, the following is obtained.

$$-\frac{\partial V}{\partial x}dx + fdx + \ P\frac{\partial P}{\partial x} + P\frac{\partial^2 w}{\partial x^2}dx + \frac{\partial P}{\partial x}\frac{\partial w}{\partial x}\cdot dx + \frac{\partial P}{\partial x}\frac{\partial^2 w}{\partial x^2}dx^2 - P\frac{\partial w}{\partial x} = \rho A dx\frac{\partial^2 w}{\partial t^2} \tag{33}$$

Since *dx* is very small and *dx* is squared, this term is negligible and becomes zero. Dividing the equation by *dx* and simplifying it, the following equation is obtained.

$$-\frac{\partial V}{\partial x} + f + \frac{\partial}{\partial x}\left(P\frac{\partial w}{\partial x}\right) = \rho A\frac{\partial^2 w}{\partial t^2} \tag{34}$$

In this term, $\frac{\partial}{\partial x}\left(P\frac{\partial w}{\partial x}\right)$, the product rule is used.

Equation (35) is now simplified.

$$(M + dM) - M - (V + dV)dx + fdx\frac{dx}{2} = 0 \tag{35}$$

$$\Downarrow$$

$$\frac{\partial M}{\partial x}dx - Vdx - \frac{\partial y}{\partial x} - \frac{\partial V}{\partial x}dx^2 + f\frac{dx^2}{2} = 0 \tag{36}$$

Higher-order terms cancel out which creates the following result:

$$\frac{\partial M}{\partial x}dx - Vdx - \frac{\partial y}{\partial x} = 0 \tag{37}$$

This means the following simple solution is obtained.

$$V = \frac{\partial M}{\partial x} \tag{38}$$

It is now known that the moment for at Bernoulli-Euler beam is writing like the following.

$$M = EI\frac{\partial^2 w}{\partial x^2} \tag{39}$$

Substituting equation (39) into equation (38) results in the following:

$$V = \frac{\partial}{\partial x}\left(EI\frac{\partial^2 w}{\partial x^2}\right) \tag{40}$$

Substitute equation (40) into equation (34) results in the following:

$$-\frac{\partial^2}{\partial x^2}\left(EI\frac{\partial^2 w}{\partial x^2}\right) + f + \frac{\partial}{\partial x}\left(P\frac{\partial w}{\partial x}\right) = \rho A\frac{\partial^2 w}{\partial t^2} \tag{41}$$

P is constant for small deflections because there is no acceleration in the axial direction, therefore *P* is taken outside of the derivative. *f* is then isolated.

$$f = \frac{\partial^2}{\partial x^2}\left(EI\frac{\partial^2 w}{\partial x^2}\right) + \rho A\frac{\partial^2 w}{\partial t^2} - P\frac{\partial^2 w}{\partial x^2} \tag{42}$$

This is the equation of motion for the axially loaded beam. The equation is simplified by assuming free vibrations of a uniform beam. This means that *EI* is constant, and *f* is zero. This results in the following equation:

$$EI\frac{\partial^4 w}{\partial x^4} + \rho A\frac{\partial^2 w}{\partial t^2} - P\frac{\partial^2 w}{\partial x^2} = 0 \tag{43}$$

Then a general solution to the equation of motion is obtained by using the separation of variables. The solution of *w* can be written as:

$$w(x,t) = W(x)T(t) = W(x)\tau e^{i\omega t} \tag{44}$$

Equation (44) is then substituted into equation (43).

$$\left(EI\frac{\partial^4 W}{\partial x^4} - \omega^2 \cdot \rho \cdot A \cdot W - P\frac{\partial^2 W}{\partial x^2}\right) \cdot \tau e^{i\omega t} = 0 \tag{45}$$

Because the term $\tau e^{i\omega t}$ cannot be equal to zero, we cancel the term.

A solution for W(x) of the form following form is assumed:

$$W(x) = ce^{rx} \tag{46}$$

Then equation (46) is substituted into equation (45).

$$(EIr^4 - \omega^2 \rho A - Pr^2)ce^{rx} = 0 \tag{47}$$

ce^{rx} is never zero so this cancels out and then the equation is divided by EI

$$r^4 - \frac{P}{EI}r^2 - \frac{\rho A \omega^2}{EI} = 0 \tag{48}$$

The characteristic equation is now found.

The characteristic equation can be solved using the quadratic formula.

$$r_{1,2}^2 = \frac{P}{2EI} \pm \sqrt{\left(\frac{P}{2EI}\right)^2 + \frac{\rho A \omega^2}{EI}} \tag{49}$$

The roots that come from r_1 will be the plus sign of equation (49).

$$r_1^2 > 0 \Rightarrow r_1 = \pm\sqrt{r_1^2} \tag{50}$$

The roots from r_2 is imaginary because of the following.

$$r_2^2 \leq 0 \Rightarrow r_2 \pm \sqrt{-r_2^2}i \tag{51}$$

The two positive roots give rise to $sinh$ and $cosh$ where the imaginary roots give rise to cos and sin functions.

We can write the shape function *W(x)* as:

$$W(x) = c_1 \cdot \cosh(r_1 x) + c_2 \sinh(\mathrm{r}_1 x) + c_3 \cos(r_2 x) + c_4 \sin{(r_2 x)} \tag{52}$$

Thereby the shape function for the axially loaded beam is found. Because the equation has 4 unknowns, c_1, c_2, c_3, c_4, four BCs are needed to solve for the four constants.

The beam model is constructed with both fixed-fixed and pinned-pinned BCs to see if the BCs make a difference in the performance of the model. In the following section, the frequency equation for the beam model with fixed-fixed BCs and the pinned-pinned BCs is found.

2.3.2.1 *Frequency equation for fixed-fixed beam*

The shape function $W(x)$ is found and can be seen in equation (53).

$$W(x) = c_1 \cdot \cosh(r_1 x) + c_2 \sinh(\mathrm{r}_1 x) + c_3 \cos(r_2 x) + c_4 \sin(r_2 x) \tag{53}$$

The beam model with fixed-fixed BCs is now taken into consideration. This means the following BCs are valid.

The deflection at both ends will be zero.

$$W(0) = 0\,, \qquad W(L) = 0 \tag{54}$$

The slope on both ends will also be zero.

$$W'(0) = 0, \qquad W'(L) = 0 \tag{55}$$

First, the BCs at $x = 0$ are used. To use the BCs, the derivative of the shape function is to be found.

$$W'(x) = c_1 r_1 \sinh(r_1 x) + c_2 r_1 \cosh(r_1 x) - c_3 r_2 \sin(r_2 x) + c_4 r_2 \cos(r_2 x) \tag{56}$$

The BCs are now applied to the shape function.

$$W(0) = c_1 \cosh(r_1 \cdot 0) + c_2 \sinh(\mathrm{r}_1 \cdot 0) + c_3 \cos(r_2 \cdot 0) + c_4 \sin(r_2 \cdot 0) = 0 \tag{57}$$

$$c_1 + c_3 = 0 \tag{58}$$

$$W(L) = c_1 \cosh(r_1 L) + c_2 \sinh(\mathrm{r}_1 L) + c_3 \cos(r_2 L) + c_4 \sin(r_2 L) = 0 \tag{59}$$

$$\begin{aligned} W'(0) = {} & c_1 r_1 \sinh(r_1 \cdot 0) + c_2 r_1 \cosh(r_1 \cdot 0) - c_3 r_2 \sin(r_2 \cdot 0) + c_4 r_2 \cos(r_2 \cdot 0) \\ & = 0 \end{aligned} \tag{60}$$

$$c_2 r_1 + c_4 r_2 = 0 \tag{61}$$

$$W'(L) = c_1 r_1 \sinh(r_1 L) + c_2 r_1 \cosh(r_1 L) - c_3 r_2 \sin(r_2 L) + c_4 r_2 \cos(r_2 L) = 0 \tag{62}$$

The four equations are now written in a matrix form.

$$\begin{bmatrix} 1 & 0 & 1 & 0 \\ \cosh(r_1 L) & \sinh(r_1 L) & \cos(r_2 L) & \sin(r_2 L) \\ 0 & r_1 & 0 & r_2 \\ r_1 \sin(r_1 L) & r_1 \cosh(r_1 L) & -r_2 \sin(r_2 L) & r_2 \cos(r_2 L) \end{bmatrix} \begin{bmatrix} c_1 \\ c_2 \\ c_3 \\ c_4 \end{bmatrix} = \begin{bmatrix} 0 \\ 0 \\ 0 \\ 0 \end{bmatrix} \tag{63}$$

The determinant of the coefficient matrix is found, and the result is then described in a simplified equation.

$$\left\|\left|\begin{bmatrix} 1 & 0 & 1 & 0 \\ cosh(r_1 L) & sinh(r_1 L) & cos(r_2 L) & sin(r_2 L) \\ 0 & r_1 & 0 & r_2 \\ r_1\, sin(r_1 L) & r_1\, cosh(r_1 L) & -r_2\, sin(r_2 L) & r_2\, cos(r_2 L) \end{bmatrix}\right|\right\| = 0 \tag{64}$$

$$\Rightarrow\ 2 r_1 r_2 (1 - \cosh(r_1) \cos(r_2)) + (r_1^2 - r_2^2) \cdot \sinh(r_1) \cdot \sin(r_2) = 0 \tag{65}$$

The equation is set equal to zero to find the non-trivial solutions and thereby the frequency equation for the beam model with fixed-fixed BC is found. Because it is not possible to find an explicit equation for the natural frequency, numerical methods are used to calculate the roots of the equation. The frequency equation obtained is used later in the study to update the physical beam model with fixed-fixed BCs.

2.3.2.2 Frequency equation for pinned-pinned beam

The physical beam model is now modelled with pinned-pinned BCs. This means that the deflection in both ends will be zero:

$$W(0) = 0\,, \qquad W(L) = 0 \tag{66}$$

The moment on both ends will also be zero

$$W''(0) = 0, \qquad W''(L) = 0 \tag{67}$$

The shape function from equation (53) is differentiated two times.

$$W''(x) = c_1 r_1^2 \cosh(r_1 x) + c_2 r_1^2 \sinh(r_1 x) - c_3 r_2^2 \cos(r_2 x) - c_4 r_2^2 \sin(r_2 x) \tag{68}$$

The four BCs in equations (66) and (67) are applied to the shape function.

$$W(0) = c_1 \cosh(r_1 \cdot 0) + c_2 \sinh(\mathrm{r}_1 \cdot 0) + c_3 \cos(r_2 \cdot 0) + c_4 \sin(r_2 \cdot 0) = 0 \tag{69}$$

$$c_1 + c_3 = 0 \tag{70}$$

$$W(L) = c_1 \cosh(r_1 \cdot L) + c_2 \sinh(\mathrm{r}_1 \cdot L) + c_3 \cos(r_2 \cdot L) + c_4 \sin(r_2 \cdot L) = 0 \tag{71}$$

$$\begin{aligned} W''(0) = c_1 r_1^2 \cosh(r_1 \cdot 0) + c_2 r_1^2 \sinh(r_1 \cdot 0) - c_3 r_2^2 \cos(r_2 \cdot 0) \\ - c_4 r_2^2 \sin(r_2 \cdot 0) = 0 \end{aligned} \tag{72}$$

$$c_1 r_1^2 - c_3 r_2^2 = 0 \tag{73}$$

$$\begin{aligned} W''(L) = c_1 r_1^2 \cosh(r_1 \cdot L) + c_2 r_1^2 \sinh(r_1 \cdot L) - c_3 r_2^2 \cos(r_2 \cdot L) \\ - c_4 r_2^2 \sin(r_2 \cdot L) = 0 \end{aligned} \tag{74}$$

The four equations are now written in a matrix form.

$$\begin{bmatrix} 1 & 0 & 1 & 0 \\ \cosh(r_1 L) & \sinh(r_1 L) & \cos(r_2 L) & \sin(r_2 L) \\ r_1^2 & 0 & -r_2^2 & 0 \\ r_1^2 \cosh(r_1 L) & r_1^2 \sinh(r_1 L) & -r_2^2 \cos(r_2 L) & -r_2^2 \sin(r_2 L) \end{bmatrix} \begin{bmatrix} c_1 \\ c_2 \\ c_3 \\ c_4 \end{bmatrix} = \begin{bmatrix} 0 \\ 0 \\ 0 \\ 0 \end{bmatrix} \tag{75}$$

The determinant of the coefficient matrix is found, and the result is then described in a simplified equation.

$$\left|\left|\begin{bmatrix} 1 & 0 & 1 & 0 \\ cosh(r_1L) & sinh(r_1L) & cos(r_2L) & sin(r_2L) \\ r_1^2 & 0 & -r_2^2 & 0 \\ r_1^2\, cosh(r_1L) & r_1^2\, sinh(r_1L) & -r_2^2\, cos(r_2L) & -r_2^2\, sin(r_2L) \end{bmatrix}\right|\right| = 0 \tag{76}$$

$$\Rightarrow \sin(r_2L)\sinh(r_1L)\,(r_1^2 + r_2^2)^2 = 0 \tag{77}$$

One of the three terms must be zero for the equation to be true. The third term, $(r_1^2 + r_2^2)^2$, cannot be zero, otherwise, the beam would move as a rigid body which is not possible with the applied BCs. If the term $\sinh(r_1L)$ should be equal to zero, r_1 must be zero which is not desired. This means the following term is left:

$$\sin(r_2L) = 0 \tag{78}$$

To satisfy this equation the following is considered:

$$r_2L = n\pi, \qquad n = 0,1,2, \dots \tag{79}$$

An equation for the natural frequency can now be found by substituting equation (49) into equation (79) [14].

$$\omega_n = \frac{\pi^2}{L^2}\sqrt{\frac{EI}{\rho A}}\left(n^4 + \frac{n^2PL^2}{\pi^2EI}\right)^{\frac{1}{2}} \tag{80}$$

An equation for the natural frequency is now obtained for the beam model with the pinned-pinned BC.

To be able to perform model updating, an expression for the axial load, *P*, is found, by solving for the axial load, *P*, in equation (80).

$$\omega_n = \frac{\pi^2}{L^2}\sqrt{\frac{EI}{\rho A}}\left(n^4 + \frac{n^2PL^2}{\pi^2EI}\right)^{\frac{1}{2}} \;\Rightarrow\; P = \frac{-EI\pi^4n^4 + \omega_n^2L^4\rho A}{L^2\pi^2n^2} \tag{81}$$

The equation for the axial load, *P*, is used later in this study to update the physical model with the pinned-pinned BCs.

2.4 Updating of physical models

As mentioned in section 1.1 model updating is performed because the output from the physical model and the measurement from the data should be as close as possible. The diagram in Figure 10 below shows the physical model updating process. This model updating process can be separated into the following four steps [11]: (1) experimental measurements and structural modelling, (2) quantity extraction and correlation analysis, (3) parameter selection for updating, and (4) minimizing the objective function.

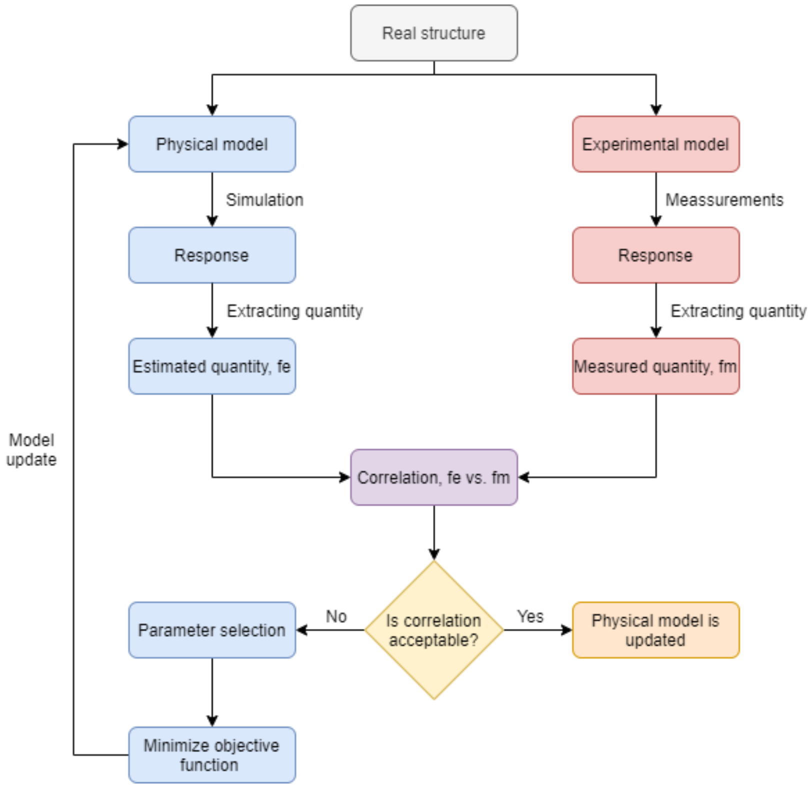

Figure 10 - Diagram of the model updating process

The experimental measurements are made based on the vibration tests from the hanger on the Great Belt Bridge, as described in section 2.2. Based on these measurements, a matrix with the samples of the response measured at the location is created. By using knowledge of the structural properties of the hanger cable, a physical model that produces outputs representative of the structure's response can be created. Often, the outputs of the model are different from the measurements, due, for example, to incorrect geometrical properties, inexact values of material properties, BCs modelled incorrectly, or difficulties in modelling damping.

If the estimated quantity from the structural model and the quantity based on measurements from the real structure does not correlate, model updating must be performed. The model is updated based on a parameter selection, where parameters that are assumed to be uncertain are chosen. The purpose of the physical models is to describe the real data from the Great Belt Bridge. Most material properties are given by Sund & Bælt, but the axial load is difficult to estimate because of the varying environmental and operational conditions. Therefore, the axial load is chosen as the updating parameter. The selected parameters are estimated by minimizing an objective function, J, with respect to the updating parameters, $\boldsymbol{p}$:

$$\min_{P} J = \big(R(\boldsymbol{p})\big)^2 = \big(\omega_{n,model}(P) - \omega_{n,measure}\big)^2 \tag{82}$$

Where $R(\boldsymbol{p})$ is the difference between the estimated quantities from the structural model and the quantities extracted from the vibration measurements, and $\omega_{n,model}(P)$ and $\omega_{n,measure}$ is the natural frequency obtained from the model and the measurements, respectively. In this study, the physical model is updated in relation to the first natural frequency from the PSD, based on the hanger monitoring data for one day, as seen in section 2.2. The model updating is performed by taking the square of the difference between the first natural frequency of the physical model, $\omega_{n,model}$, and the first natural frequency of the measured data, $\omega_{n,measure} = 0.39\ Hz$, and by this find the axial load, P, that results in the smallest difference. For the fixed-fixed beam model, the objective function is non-linear with respect to the updating parameters, hence the minimization must be done by optimization algorithms [16]. The optimization is made in MATLAB with the function “fminbnd”. “fminbnd” finds a minimum for a problem in a specified region. In this study, the “fminbnd” seeks to minimize the objective function that has been made. In this case, the objective function consists of the error between the measured natural frequency and the model predicted natural frequency which can be seen in equation (82). The default setting for “fminbnd” is used which means that the optimization runs a maximum of 500 function evaluations and a maximum of iterations and uses a tolerance of 10^{-4}.

2.4.1 Updating of string model and pinned-pinned beam model

In the model for the string and the pinned-pinned beam in sections 2.3.1.1 and 2.3.2.2, respectively, an explicit equation for the natural frequency is found. This means that expressions for the axial load, P, can be found by solving, as seen in equation (26) for the string model and equation (81) for the pinned-pinned beam model. These two equations are used to conduct the model updating for the two models by inserting the first natural frequency of $\omega_{measure} = 0.39\ Hz$ from the PSD-plot in Figure 5. By this, the axial load corresponding to the measured natural frequency is found and model updating is performed.

2.4.2 Updating of fixed-fixed beam model

It is not possible for the fixed-fixed beam, to use “fminbnd” directly because an equation for the natural frequency cannot be obtained explicitly. The natural frequency for the fixed-fixed beam can be obtained by using the Newton-Raphson method and a line search. The line search is used to find an initial point that has to be used in the Newton-Raphson method. The Newton-Raphson method is an iterative process that finds the point where the function crosses the *x*-axis. The method requests an initial guess and then calculates the first point with the following equation.

$$x_1 = x_0 - \frac{f(x_0)}{f'(x_0)} \tag{83}$$

This point is then used to find the next point and the general equation for finding the next point is the following:

$$x_{n+1} = x_n - \frac{f(x_n)}{f'(x_n)} \tag{84}$$

In this way, the method approaches the intersection between the function and the *x*-axis. In this study, the Newton-Raphson method is used to find the root of the frequency equation. The frequency equation and the derivative are not calculated separately. Instead, the ratio is calculated directly to ensure that the value of the frequency equation and the derivative do not become too large and result in numerical problems. In this way, a value for the natural frequency is obtained and this can be substituted into the objective function described in section 2.4 and a value for the axial load can be obtained.

3 Results and interpretation

In the following sections, the results and the interpretation of these results are presented.

3.1 Natural frequencies and mode shapes

First, the obtained values for the natural frequencies and mode shapes are investigated. The frequency equations for each of the three physical models are plotted, as seen in Figure 11. The natural frequencies for each model in the table are based on the initial assumption that the axial load, *P*, is 10,000,000 N. Based on the plots of the characteristic equations for the eigenvalues, peak picking is completed, which also is shown in Figure 11 below.

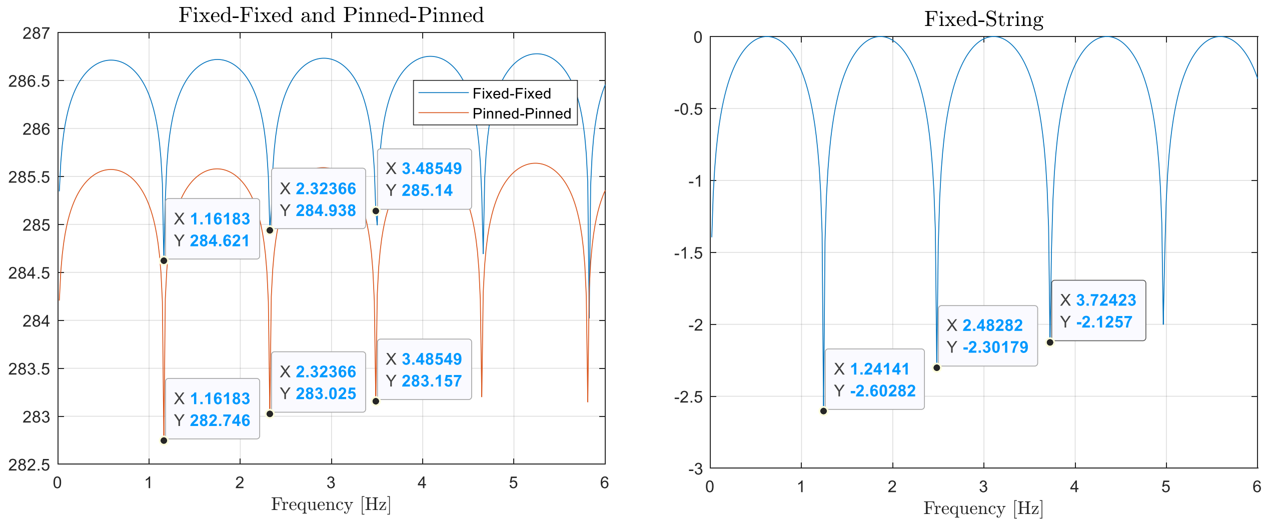

Figure 11 - Plots of the characteristic equations for the eigenvalues for the three physical models before model updating

Table 3 below contains the natural frequencies for the three physical models based on the completed peak picking from Figure 11 above.

Table 3 - First natural frequency for the three physical models

	Fixed string	Beam pinned-pinned	Beam fixed-fixed
First natural frequency	1.241 Hz	1.161 Hz	1.161 Hz

As seen in section 2.2, a PSD is made based on the hanger monitoring data from Sund & Bælt. From this PSD, the first natural frequency is read to be 0.39 Hz. The first natural frequency from the three physical models in Table 3 and the first natural frequency from the hanger monitoring data differ a lot, therefore, model updating is conducted, as stated in section 2.4.

Figure 12 below shows the frequency plot of the three physical models after model updating was completed. The updated axial loads used for the plots of the characteristic equations for the eigenvalues in Figure 12 are shown in Table 4.

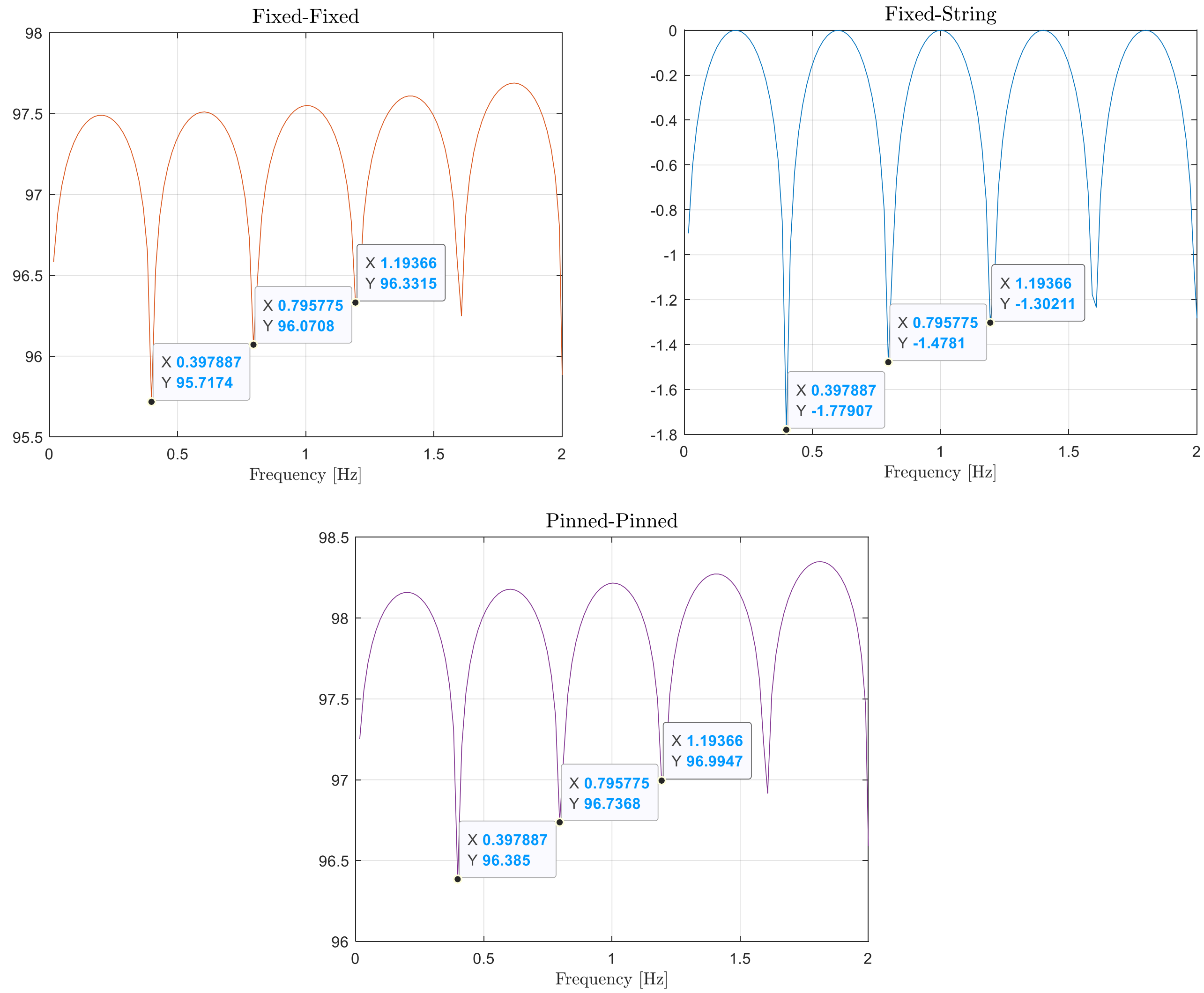

Figure 12 - Plots of the characteristic equations for the eigenvalues for the three physical models after model updating

From the three plots of the characteristic equations for the eigenvalues in Figure 12 above, it is seen that the natural frequencies now are approximately the same as the natural frequencies from the hanger monitoring data. This means that the model is updated correctly. After looking at the natural frequencies the mode shape for the three physical models is investigated.

In Figure 13 below, the mode shapes for the three different physical models are shown. The mode shapes are plotted on basis of the shape function for each of the three models. The shape function for the fixed-string model, the fixed-fixed model, and the pinned-pinned model can be seen in equations (17) and (52) respectively.

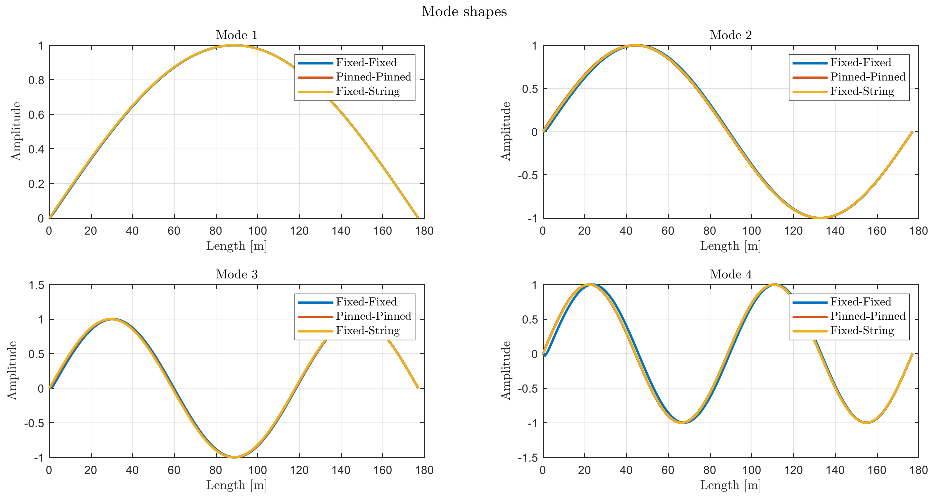

Figure 13 - Mode shapes for the three different physical models

The form of the mode shapes for each of the three physical models are the same. It was expected that there would be a visual difference between especially the fixed-fixed and pinned-pinned mode shapes, but there is not. The most likely explanation for this is that the stay cable has a length such as it would not affect the mode shape.

3.2 Axial Load

Next, the axial loads obtained by the model updating are investigated. After model updating is conducted as described in section 2.4, the following axial loads for each of the three physical models are obtained. The axial values obtained from the three models can be seen in Table 4.

Table 4 - Axial load for the three physical models

	String Fixed-Fixed	Beam Pinned-Pinned	Beam Fixed-Fixed
Axial load	$1.03 \cdot 10^6$ N	$1.19 \cdot 10^6$ N	$1.17 \cdot 10^6$ N

All the obtained axial loads are in the same range which substantiates that the actual axial load should have a magnitude around this range. From the obtained axial loads it can be concluded that the most conservative model is the beam model with the pinned-pinned BC. This could be a reason for choosing the beam model with pinned-pinned BCs. The string model results in the lowest axial load and it is also considered the least accurate model. The reason for this is that even though it is possible to model cables as strings they do not take the bending stiffness into account. Because there is no bending stiffness many cables have failed due to fatigue caused by alternating bending. The alternating bending is produced by the regular shedding of vortices from the cable in light wind [14]. Therefore, the string model will not be the best-suited model for the purpose of monitoring the cable loads. To verify that the axial loads found are in a reliable range it is investigated which size of the axial load is obtained if the bridge deck is a solid concrete block and not a hollow bridge deck as it is. It is assumed that the load is evenly distributed. The bridge is 31 m wide and 2694 m long with 212 hanger pairs. The distance between the hanger pairs is found.

$$d = \frac{2694\ m}{212} = 12.708\ m \tag{85}$$

The distance between two hanger pairs is $12.708\ m$. Because it is assumed that the load is evenly distributed the size of the concrete block, used to review P, has to be $12.708\ m$ long, and the half of the width, which is $15.5\ m$, and $4\ m$ high [17].

$$\begin{aligned} m_{concrete\ block} &= \rho_{concrete\ block} \cdot L \cdot w \cdot h = 2.4 \frac{g}{cm^3} \cdot 12.708m \cdot 15.5m \cdot 4m \\ &= 1891\ tons \end{aligned} \tag{86}$$

The axial force the cable must carry is found by multiplying the mass of the concrete block with the gravitational force.

$$P_{axial,concrete} = 1891\ tons \cdot 9.82 \frac{m}{s^2} = 18{,}6\ MN \tag{87}$$

This axial load is divided by two because the hangers are in pairs and the load should only be for one cable.

$$P_{axial,concrete} = \frac{18{,}6}{2}\ MN = 9{,}3\ MN$$

This means that if the mass the stay cable has to carry had been solid concrete it would have resulted in a higher axial force because the axial loads for the three physical models are lower as seen in Table 4. This substantiates that the axial load found from the optimization is coherent with the physical dimensions of the bridge, as the mass the stay cable must carry is a hollow bridge deck which would be a smaller mass than a solid concrete block.

3.3 Comparison of the three physical models

At last, a comparison of the three physical models is made. This is done by plotting the three physical models' natural frequencies as a function of the axial load. The plot can be seen in Figure 14 below.

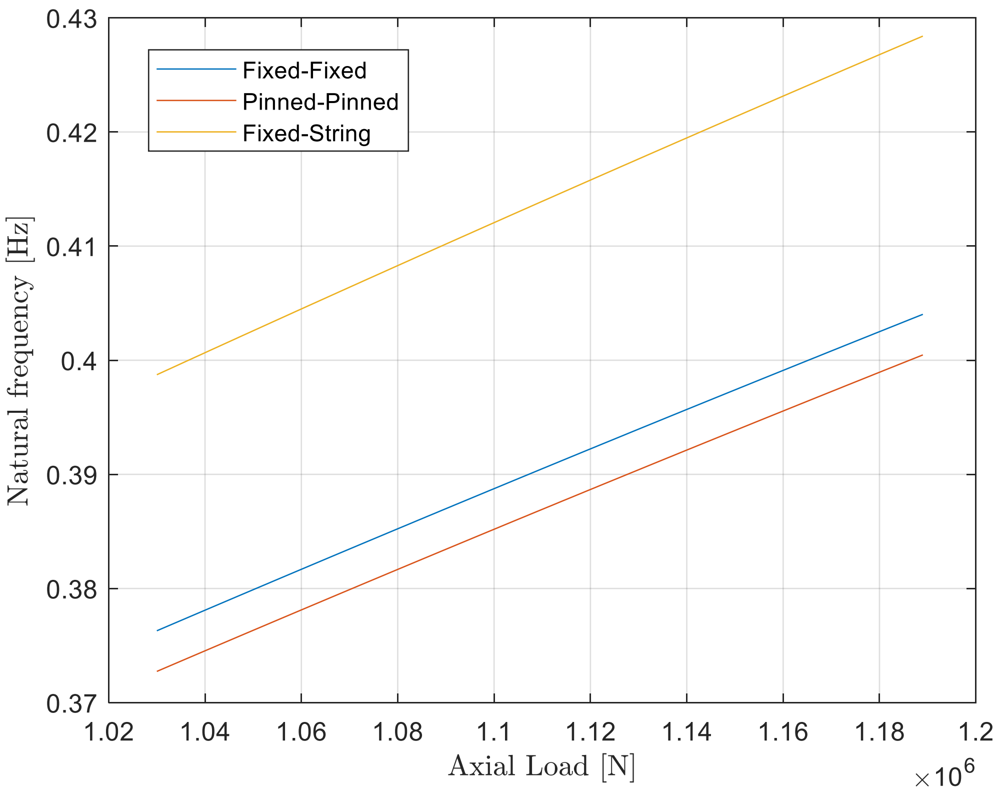

Figure 14 - Natural frequencies obtained with each one of the physical models plotted as a function of the axial load

From Figure 14 it can be concluded that all three physical models have the same trend because all three models indicate that they can be described as linear functions. The physical models having the same trend are what was desired. It was desired because the three physical models having the same trend means that the three models agree on how to model the structure. The graphs for the three models have an offset in relation to each other. This is also the reason why the three physical models result in three different axial loads at the same frequency, which also can be seen in Figure 14.

To ensure the three models have the exact same trend, the slope and intercept of each physical model are found. The slopes and intercepts can be seen in Table 5.

Table 5 - Slope and intercepts for the three physical models

	String Fixed-Fixed	Beam Pinned-Pinned	Beam Fixed-Fixed
Slope [Hz/N]	0.207	0.193	0.197
Intercept [Hz]	$1.87 \cdot 10^{-7}$	$1.74 \cdot 10^{-7}$	$1.74 \cdot 10^{-7}$

The slopes are not identical, but similar. The slope of the string model stands out the most, but this model is already rejected as a model due to the lack of bending stiffness. The slopes of the beam models only have a difference of 1.8%. Therefore, it is possible to conclude that the two beam models have the same trend. The two beam models having the same trend are convenient because then the offset can be utilized to switch from one model to the other with a deterministic correction. This means that it is possible to do the calculations with the pinned-pinned beam model and then with the known offset switch the calculations into the fixed-fixed model. Therefore, there is no reason to choose the fixed-fixed beam model to represent the best-suited physical model for the purpose of monitoring the cable loads compared to the pinned-pinned beam model.

4 Future work

If the work of this study should be continued and elaborated on, there would be some interesting subjects to look at. These subjects are described in this section.

First, in this study, the reference natural frequency is extracted from the dataset for one day. It would be interesting to explore if this natural frequency changes if the dataset were from multiple days or days with different weather conditions. This is relevant because if the reference natural frequency change, the model updating will also give different results.

Second, the hanger cables on the Great Belt Bridge consist of two coupled hanger cables. In this study, the physical models are modelled as one cable even though the hanger cables are coupled. Around the fourth natural frequency, it becomes clear in the PSD that peak splitting is present. This is most likely because the hanger cables consist of a pair of cables and therefore would be interesting to investigate more.

Third, it would be interesting to study the effect of wind loads on the hanger cables. The wind loads are not expected to have a significant effect in the present analysis, but it is worth studying to ensure all aspects are taken into consideration.

Last, the BCs used for the physical model in this study are pinned-pinned and fixed-fixed. It would be interesting to investigate the results of the physical model if the BC were pinned-fixed because it seems to be the most correct BC if the actual structure is taken into consideration.

5 Conclusion

To establish a model updating strategy that can be used for monitoring the hanger cable loads in the Great Belt Bridge, three different physical models representing the vibration response of the hanger cables of the Great Belt Bridge in normal operational conditions are developed. The three physical models consist of a string model with fixed BCs, and a beam model with pinned-pinned and fixed-fixed BCs.

For the beam model with fixed-fixed BCs, an iterative non-linear optimization method with the natural frequencies as the characteristic quantities is used for the model updating. The updating parameter is the axial load, P, because due to varying environmental and operational conditions, this parameter is difficult to estimate. For the string model and the pinned-pinned beam model, the model updating is performed by solving for the axial load, P, directly. The updated results have shown that the updated physical model of the structure agrees well with the actual model.

If the wrong model or BCs are chosen it could result in a wrong estimation of parameters but also a wrong estimation of fatigue life, which could lead to catastrophic incidents. Therefore, a comparative analysis of the three models is conducted, and a plot showing the natural frequency as a function of the axial load is illustrated. Based on this plot, it is seen that the trend is approximately the same for the three physical models, making it possible to switch from one model to the other with a deterministic correction.

Based on this comparative analysis, it is concluded that the simplest model, in relation to computational effort, can be chosen as the best-suited physical model. The simplest model regarding computational effort is the string model, but because the bending stiffness is not present in this model, it is deselected. The simplest model of the two beam models is the beam model with the pinned-pinned BCs, therefore, and because of the potential to use deterministic correction, this model is chosen as the best-suited physical model for the purpose of developing a Structural Health Monitoring strategy for the hanger cables.

6 References

[1] Guo, N., Yang, Z., Wang, L., Ouyang, Y., and Zhang, X., 2018, "Dynamic model updating based on strain mode shape and natural frequency using hybrid pattern search technique," Journal of Sound and Vibration, 422, pp. 112-130.
[2] Zhang, L., Brincker, R., and Andersen, P., "An overview of operational modal analysis: Major development and issues," Proc. Proceedings of the 1st International Operational Modal Analysis Conference, IOMAC 2005.
[3] Pedram, M., Esfandiari, A., and Khedmati, M. R., 2017, "Damage detection by a FE model updating method using power spectral density: Numerical and experimental investigation," Journal of Sound and Vibration, 397, pp. 51-76.
[4] Prendergast, L. J., Wu, W. H., and Gavin, K., 2019, "Experimental application of FRF-based model updating approach to estimate soil mass and stiffness mobilised under pile impact tests," Soil Dynamics and Earthquake Engineering, 123, pp. 1-15.
[5] Bhargava, C., 2020, AI Techniques for Reliability Prediction for Electronic Components, IGI Global.
[6] Pratihar, D. K., 2012, Computational Optimization and Applications, Narosa Publishing House Pvt. Ltd.
[7] MathWorks, 2022, "What Is Direct Search?," https://se.mathworks.com/help/gads/what-is-direct-search.html?fbclid=IwAR2KeYyLXiuyRhxazLshRn7hRhgF5she7sgPlA7KvWC6bDCy9yLAVHsJPBU.
[8] Chang, K.-H., 2014, Design Theory and Methods using CAD/CAE - The Computer Aided Engineering Design Series, Academic Press.
[9] Galvan, B., Greiner, D., Périaux, J., Sefrioui, M., and Winter, G., 2003, "Parallel evolutionary computation for solving complex CFD optimization problems. A review and some nozzle applications," Parallel Computational Fluid Dynamics 2002: New Frontiers and Multi-Disciplinary Applications, pp. 573-604.
[10] Alkayem, N. F., Cao, M., Zhang, Y., Bayat, M., and Su, Z., 2018, "Structural damage detection using finite element model updating with evolutionary algorithms: a survey," Neural Computing and Applications, 30(2), pp. 389-411.
[11] Marwala, T., 2010, Finite-element-model Updating Using Computional Intelligence Techniques - Applications to Structural Dynamics, Springer.
[12] Park, G., Hong, K. N., and Yoon, H., 2021, "Vision-based structural fe model updating using genetic algorithm," Applied Sciences (Switzerland), 11(4), pp. 1-16.
[13] Ribeiro, D., Calçada, R., Brehm, M., and Zabel, V., 2021, "Calibration of the numerical model of a track section over a railway bridge based on dynamic tests," Structures, 34, pp. 4124-4141.
[14] Rao, S. S., 2018, Mechanical Vibrations, Pearson Education, Inc.
[15] Freeball, G. V. w., 2020, "Transverse Vibration Analysis of an Axially-Loaded Euler-Bernoulli Beam (Continuous System)," https://www.youtube.com/watch?v=gETXbAA_808&ab_channel=GoodVibrationswithFreeball.
[16] Kerschen, G., Worden, K., Vakakis, A. F., and Golinval, J. C., 2006, "Past, present and future of nonlinear system identification in structural dynamics," Mechanical Systems and Signal Processing, 20(3), pp. 505-592.
[17] Structurae, 2022, "Great Belt East Bridge," https://structurae.net/en/structures/great-belt-east-bridge?fbclid=IwAR3_oeuX7kuQ8xGwuN0PQQCtQqSI6Ds0WpZ_y_HYYbUrCuOTj2xlKSxnFHo.